Journal of Cleaner Production 274 (2020) 123260

Contents lists available at ScienceDirect

Journal of Cleaner Production

journal homepage: www.elsevier.com/locate/jclepro

Iron ore tailings as a supplementary cementitious material in the production of pigmented cements

Luciano Fernandes de Magalhães [a], Sâmara França [a], Michelly dos Santos Oliveira [a], Ricardo André Fiorotti Peixoto [b], Sofia Araújo Lima Bessa [c], Augusto Cesar da Silva Bezerra [a, *]

[a] Federal Center for Technological Education of Minas Gerais, Belo Horizonte, MG, 30421-169, Brazil
[b] Dept. of Civil Engineering, Federal University of Ouro Preto, Ouro Preto, MG, 35400-000, Brazil
[c] Federal University of Minas Gerais, Belo Horizonte, MG, 31270-901, Brazil

ARTICLE INFO

Article history:
Received 22 September 2019
Received in revised form
9 April 2020
Accepted 27 June 2020
Available online 17 July 2020

Handling editor Prof. Jiri Jaromir Klemeš

Keywords:
Iron ore tailings
Pigment
Portland cement
Durability
Sustainability

ABSTRACT

In this paper, the characterisation of iron ore tailings (IOT) was carried out to examine its use as a supplementary cementitious material (SCM) to produce coloured composite cements. The IOT was heat treated, and ten different mixtures were prepared, substituting Portland cement for 10, 20 and 30 wt%. The IOT presented the sum of oxides of silicon, aluminium and iron higher than the minimum prescribed in Brazilian and international standards to be considered a pozzolanic material. The grain size of the IOT was smaller than the grain size of the Portland reference cement and met the standards used. The electrical conductivity indicated that all IOTs are pozzolans, and the index of pozzolanic activity indicated that the heat treatment at 750 °C transformed the IOT into pozzolan. The heat treatment changed the colour of the IOT, and that influenced the colour of the composite cement with IOT and in turn, the colour of the produced mortars. In the IOT without thermal treatment, the presence of the kaolinite mineral was identified, and the thermal treatment led to the non-identification of this mineral, probably transforming it into an amorphous phase. The thermogravimetric analysis confirmed the transformation of kaolinite into metakaolinite. The compressive strength presented by IOT composite cement was adequate for several commercial cements provided for in Brazilian and in international standards. Cement with IOT showed lower values de loss of mass and microstructure with less damage under acid attack, and this behaviour was optimized with increases in the percentage and temperature of IOT heat treatment. Finally, the synergy between milling and heat treatment optimized the use of IOT as a pozzolan capable of changing the colour of the final cementitious product, as well as its use as an SCM.

1. Introduction

Portland cement forms the base of concrete production; it is the most commonly used structural material in the world and has enormous applications in residential, commercial and industrial areas (Imbabi et al., 2012; Scrivener et al., 2018; Ghalehnovi et al., 2019; Yadav et al., 2019; Amran et al., 2020). Portland cement is produced by the calcination of lime and clays, and the calcination of lime releases considerable amounts of carbon dioxide (CO_2). While CO_2 emissions per ton of Portland cement are decreasing, the cement industry's CO_2 emissions are becoming increasingly worrying as cement consumption around the world is steadily increasing. Cement production is estimated to account for 5–8% of total global CO_2 emissions (Díaz et al., 2017; Scrivener, 2014). Concerns over these emissions have resulted in new alternatives being adopted to produce low-carbon cement, where supplementary cementitious materials (SCM) are used to replace Portland cement clinker (Scrivener et al., 2018). The production of Portland cement clinker requires thermal input at temperatures of approximately 1500 °C (Scrivener et al., 2018; Bhagath Singh and Subramaniam, 2019), while for SCM from residual soils or

Abbreviations: SCM, Supplementary Cementitious Materials; IOT, Iron Ore Tailings.

* Corresponding author.
E-mail addresses: luciano_fm8@hotmail.com (L.F. Magalhães), samara_franca@yahoo.com.br (S. França), michelly@cefetmg.br (M.S. Oliveira), ricardofiorotti@ufop.edu.br (R.A.F. Peixoto), sofiabessa@ufmg.br (S.A.L. Bessa), augustobezerra@cefetmg.br (A.C.S. Bezerra).

https://doi.org/10.1016/j.jclepro.2020.123260
0959-6526/

biomass, commonly, there is no requirement for the temperature to exceed 800 °C (Bezerra et al., 2017; Scrivener et al., 2018; Yadav et al., 2019). Additionally, the benefits of using SCM may include the improvement of the mechanical properties, decreasing on the porosity, permeability and deleterious reactions (Paris et al., 2016), and different physical properties such as pigmentation (Galvão et al., 2018).

The SCM commonly used are wastes from industrial sectors, such as blast furnace slag, fly ash, silica fume, waste glass, and residues of ceramic industry (Puerta-Falla et al., 2015; Keppert et al., 2017; Záleská et al., 2018a). Another industrial by-product with potential for use as an SCM is biomass, materials of organic origin. Several authors have investigated the replacement of cement by ash from wood burning in thermoelectric and sugarcane bagasse plants, obtaining composites with mechanical properties compatible with current standards, as well as reducing the amount of CO_2 (15–20%) and energy (11–16%) (Bezerra et al., 2017; Salvo et al., 2015; Sklivaniti et al., 2017; Pavlíková et al., 2018). Záleská et al. (2018b) investigated the use of sewage wastewater treatment sludge, noticing pozzolanic activity of this material in cementitious composites. Jankovský et al. (2017) studied wheat straw ashes and found high pozzolanic activity. Rahhal et al. (2019) studied ceramic waste originated in a ceramic factory and concluded that it could be used as a pozzolanic material contributing to the reduction of CO_2 emission in cement-based materials. Bezerra et al. (2019) obtained a cementless binder from the alkaline activation of biomass from the burning of eucalyptus chips and iron ore tailings, aiming to incorporate the composite into building materials.

Calcined clays are prominent SCM, especially those with high kaolinite contents (±40%). The world reserves of clays are vast and represent an enormous potential SCM supply (Scrivener, 2014). However, despite the reduction in the impact of Portland cement production, which is quite huge for the sector, the use of calcined clay as an SCM demands the extraction of these clays in the environment, which may require interventions, such as some deforestation, movement of soil, cuts and landfills. The use of clays that did not require further intervention would further reduce the impact of cement production. The possibility of using residual clays from the mineral mining processes seems promising.

Iron ore tailings (IOT) are materials that may contain clay minerals. Iron is the fourth most abundant element in the Earth's crust and is the primary raw material of steel, which is the most consumed metal alloy in the world (Shettima et al., 2016). The high demand for iron resulted in the mining of ores with lower iron contents, which led to increasing the waste generation (Guimaraes et al., 2012). On a worldwide scale, this number increased to 2230 billion tons, with 1360 billion tons of this total being material with the potential to be reused. The world production of IOT in 2016 was led by Australia, at approximately 825 Gt, followed by Brazil (391 Gt) and China (353 Gt) (U.S. Geological Survey, 2017). This large volume of this material is usually disposed of in the form of tailing dams (Bastos et al., 2016; Pappu et al., 2007).

These dams can directly impact the environment due to the large volumes of material in the dams, with social and environmental impacts in the event of a failure (Passos et al., 2017). Therefore, dam safety is considered a great challenge for engineers. In recent decades, accidents have occurred and devastating ecosystems and killed hundreds of species (Aires et al., 2018). In 1998, a dam burst in Aznalcollar, Spain and released 2 million m^3 of tailings into the environment, resulting in contamination of aquifers and surface water and also the death of several aquatic species (Davies, 2002). In 2003, the largest disaster of this type occurred in the Republic of Macedonia and released 100,000 m^3 of tailings with heavy metals into the Kamenica River. The tailings wave reached approximately 10 m in height and 12 km in length (Vrhovnik et al., 2013). In 2008, an IOT dam accident occurred in Shanxi Province, China, causing 277 deaths and $14.59 million in economic losses (Ke et al., 2016; Yang et al., 2017; Yao et al., 2019a, 2020).

In Brazil, recent cases of dam failure have shown the devastating consequences of the collapse of these structures. In 2015, a dam that stored IOT in Mariana (Minas Gerais state) failed and dumped approximately 62,000,000 m^3 of tailings that travelled 663 km along three rivers to the mouth of the Atlantic Ocean, thus affecting aquatic species and damaging the water supplies of several communities (Lacaz et al., 2017). In 2019, a dam failed in Brumadinho (Minas Gerais state) that also stored IOT, releasing approximately 12,700,000 m^3 of tailings and leaving 259 dead and 11 missing (Cavallini, 2019; Minas Gerais, 2019; VALE, 2019). Also, mining tailings are generally related to a reduction in organic soil matter and nutrients (Lange et al., 2012), and acidification due to the increase in pH (Chaturvedi et al., 2014), decreased permeability (Mouazen et al., 2014), increased density (Sakai et al., 2008) and increased salinity (Li et al., 2014).

Due to the impacts of IOT disposal, several studies have investigated the potential of this material for reuse. Zhang et al. (2011) showed that IOT had great potential for use in civil construction using the geopolymerization technique. Huang et al. (2012) concluded that the replacement of cement with IOT could lead to a reduction in energy consumption of approximately 32% and a reduction in greenhouse gas emissions of approximately 63% in the manufacture of cementitious composites. Kuranchie et al. (2015) studied IOT as a concrete aggregate and obtained an increase in compressive strength of 11% compared with those concretes with natural aggregates. Bastos et al. (2016) investigated the potential of IOT as a material for infrastructure. Neto et al. (2014), Morais et al. (2018) and Magalhães et al. (2018) used thermally treated mining waste to partially replace clinker and concluded that this alternative could produce cement with adequate strength. Cui et al. (2017) used IOT in autoclaved aerated concretes.

In addition to having potential as SCM, precursors for geopolymerization, and aggregates, IOT has demonstrated potential as a pigment due to its chemical composition (Galvão et al., 2018). Fontes et al. (2018) used IOT from dams to replace aggregates in the fabrication of roof tiles and as a pigment and concluded that this material could be possibly used for this purpose because the IOT may lead to homogeneous colour products. The pigments most used for the pigmentation of cementitious composites are inorganic pigments, which are composed with oxides, mainly iron oxides, that provide raw materials to produce red, yellow, black and brown pigments (Hospodarova et al., 2015). Inorganic pigments are liquids or powders. The use of liquid pigments in concrete does not affect the physical properties, such as mechanical strength or porosity (Hospodarova et al., 2015); however, powder pigments may reduce the workability of concrete due to the increased surface area in the system (Lee et al., 2005).

In this scenario, the use of IOT as supplementary cementitious material to produce Portland cement with different pigments, adding value to the product, reducing the environmental impact inherent to the disposal of this material in dams and determining a large-scale method of immobilisation/encapsulation of IOT in a cement matrix was investigated.

2. Materials and methods

2.1. Materials

For the development of this work, the following materials were used: samples of iron ore tailings (IOT), Brazilian standard sand, reference Portland cement (portland-cement clinker (~95 wt%) and

calcium sulfate (~5 wt%)) and water.

2.1.1. Iron ore tailings (IOT)

The samples of IOT were collected from the thickeners, which generates a finer material than the tailings from the high-frequency screens; it also passed through a filter press. As the collected waste was not disposed of in a dam, it presents some uniformity in the mineralogical composition. Thus, sample collection was performed randomly at various points in the tailings pile.

tIOT was collected with humidity of 14% and dried in an oven at 105 °C for 24 h. After drying the sample, thermogravimetric analysis was performed to define the temperatures the unground IOT would be subjected to in the thermal treatment. The thermogravimetric analysis (TGA) on SHIMADZU DTG - 60H thermal equipment using platinum crucible with heating rate 5 °C.min^{-1}, operated with nitrogen gas at 100 mL min^{-1} and temperature variation between 24 °C and 1100 °C, used 5 mg of sample. To highlight the influence of sample collection on thermal analysis, the assay was performed three times for the unground IOT, and no differences were found in the results that changed no more than 0.1% of the percentage mass loss per temperature range analyzed. The largest mass loss gradients observed in the unground IOT sample without heat treatment were 5.5% and 1.0% at temperatures of approximately 500 °C and 750 °C, respectively. Thus, temperatures of 500 °C and 750 °C were used for the thermal treatment, which was performed in an industrial rotary oven at 2 rpm for 40 min. After the thermal treatment, all samples of IOT were ground and named WHT (without heat treatment and ground), HT 500 (with heat treatment at 500 °C and ground) and HT 750 (with heat treatment at 750 °C and ground). The IOT was ground in a Pulverisette Fritsch planetary mill at 300 rpm for 10 min in 250-g portions in 500-ml bowls with 18 20-mm spheres. IOT grinding was used to improve reactivity, as it may induce changes in the physical and chemical properties of particles, such as particle size, crystalline structures and surface properties (Yao et al., 2019a, 2020).

After grinding, thermal analysis was performed again with WHT, HT500 and HT750 samples. The particle size distribution was determined using a Cilas 1090 Laser Particle Size Analyzer. The particle size analysis was performed wet, using distilled water as a liquid. The samples were individually added in the sample bath with centrifugal pump and agitator turned on until the obscuration of 15% was obtained. After obtaining the desired obscuration, the ultrasonic probe was turned on for 60 s and the particle size measurement was performed. The chemical composition was determined by X-ray fluorescence using pellets fused with lithium tetraborate and a Panalytical X-ray fluorescence spectrometer. The X-ray diffraction was performed with a Shimadzu XRD-7000 diffractometer operating with Cu K-alpha radiation (40 kV/30 mA), with 2Θ from 10° to 80° at a step of 2°/min. The peaks were identified using the software Match! 3 with the Crystallography Open Database (COD) revision no. 211633.

2.1.2. Brazilian Standard Sand

Brazilian Standard Sand for cement tests was provided by the Technological Research Institute (IPT-SP), according to the specifications provided by Brazilian standard NBR 7214 (ABNT, 2015). Four standard fractions (retained on the sieve) were used: coarse (1.2 mm−2.4 mm), medium-coarse (0.6 mm−1.2 mm), medium-fine (0.3 mm−0.6 mm), and fine (0.15 mm−0.3 mm), with silica content (in mass) above 95%.

2.1.3. Reference Portland cement

The reference Portland cement for this work was produced with portland-cement clinker (~95 wt%) and calcium sulfate (~5 wt%), aiming to represent a Portland cement without additions, similar to CEM I of the European norm EN 197-1 (EN, 2000), which allows a maximum of 5% of minor additional constituents. The reference Portland cement had its chemical composition and particle size determined by the same procedures and equipment used for IOT.

2.1.4. Evaluation of the pozzolanicity

The work used two methods to evaluate the pozzolanicity of IOT: the pozzolanic activity index and the electrical conductivity measurement. The pozzolanicity of the IOT with and without heat treatment was quantified. According to the Brazilian standard NBR 5752 (ABNT, 2014a) for the determination of the pozzolanic activity index (I%) two mortars with two different dosages should be prepared. Mortar A should contain Portland cement composed of carbonate material, Brazilian standard sand and water. Mortar B should contain 25% by weight of pozzolanic material, replacing the equal percentage of Portland cement composed of carbonate material, Brazilian standard sand and water. The Pozzolanic activity index was calculated according to Brazilian standard NBR 5752 (ABNT, 2014a) using equation (1):

$$I\,(\%) = \frac{I_{cB}}{I_{cA}} * 100 \quad (1)$$

Where I_{cA} is the compressive strength of the control mortar (Mortar A) at 28 days, I_{cB} is the compressive strength of the mortar with the replacement of cement by pozzolanic materials at 28 days (Mortar B) and I (%) is the pozzolanic activity index. Both mortars (Mortar A and Mortar B) have a binder/aggregate ratio of 3 and a water/cement ratio of 0.48. For each mortar, four specimens were moulded, as prescribed by Brazilian standard NBR 5752 (ABNT, 2014a). The mortars for the determination of the pozzolanic activity index were produced with a Portland cement composed of carbonate material. According to the Brazilian standard NBR 16697 (ABNT, 2018), this cement is composed of clinker + calcium sulfate with percentages between 75 and 89, and carbonate material with percentages ranging from 11 to 25. According to this same standard, carbonate material is a finely ground material, consisting mostly of calcium carbonate.

The reactivity of IOT was also evaluated based on the variation in the electrical conductivity (ΔC) in a saturated calcium hydroxide solution (Luxán et al., 1989). The saturated calcium hydroxide solution used was prepared with deionized water and $Ca(OH)_2$ with 95% minimum purity. The solution was obtained by mixing and stirring the Ca $(OH)_2$ in excess with deionized water for 20 min at 500 rpm. Subsequently, the solution was kept at rest for 30 min, and eventually, the solution was filtered (Villar-Cociña et al., 2019). Each test was performed with 5 g of the IOT sample in 200 ml of the constantly stirred saturated, and filtered calcium hydroxide solution and the test temperature was maintained at 40 °C (Katare and Madurwar, 2020). The conductivity of the solution was initially measured under these conditions with an Akrom KR30 conductivity meter. Then 5 g of the IOT sample was added to the calcium hydroxide solution, keeping the mixture stirring for 120 s and the conductivity measured again after that time. The materials may be classified as non-pozzolanic when $\Delta C < 0.4$ mS cm^{-1}, as a variable pozzolanicity if 0.4 mS cm^{-1} $< \Delta C <$ 1.2 mS cm^{-1}, and as a good pozzolanic if $\Delta C >$ 1.2 mS cm^{-1} (Luxán et al., 1989). According to Villar-Cociña et al. (2019), this method allows following the variation of the electrical conductivity (ΔC) of the calcium hydroxide-pozzolan solution with the reaction time. The use of methods based on the electrical conductivity of an aqueous suspension of pozzolan/CH has significantly reduced the times needed to characterize these materials from the perspective of pozzolanicity.

2.2. Blended cement production and characterisation

IOT with and without thermal treatment were used to produce Portland cement at percentages of 0, 10, 20 and 30 wt%, as replacement of reference Portland cement (portland-cement clinker (~95 wt%) and calcium sulfate (~5 wt%)). The standard mortars were composed by aggregate/binder ratio of 3 by mass, and a water/cement ratio of 0.48 according to Brazilian Standard NBR 7215 (ABNT, 2019). This Brazilian Standard deals with the determination of the Portland cement strength class and prescribes the production of the mortar mentioned in the previous sentence for compressive strength tests. The composition of studied composites is summarized in Table 1.

For each replacement percentage, cylindrical test specimens measuring 50 mm in diameter and 100 mm in height were moulded, with five specimens produced for compressive strength test, three specimens produced for water absorption testing, porosity, bulk density (dry and saturated), and apparent density, and three specimens for acid attack test. The specimens were cured immersed in saturated water with calcium hydroxide and were ruptured at the ages of 3, 7, 28 and 90 days. The format of the cast and cure conditions are also described in the Brazilian Standard NBR 7215 (ABNT, 2019). For rupturing, an EMIC universal testing machine and the software TESC and Vmaq were used, with an increasing stress rate of 0.25 MPa/s. The sand used for cement tests is the Brazilian standard NBR 7214 (ABNT, 2015).

The flow test was performed in the fresh state, according to Brazilian Standard NBR 7215 (ABNT, 2018). The flow table and accessories provided by Brazilian Standard NBR 7215 (ABNT, 2018) for determining the flow of Brazilian standard mortar is like the devices provided by ASTM C230 (ASTM, 2014). The method proposed by the Brazilian Standard NBR 7215 (ABNT, 2018) differs from ASTM C1437 (ASTM, 2015) in the number and time of drop. Brazilian Standard NBR 7215 (ABNT, 2018) prescribes that the table be dropped 30 times in 30 s instead of 25 times in 15 s prescribed by ASTM C1437 (ASTM, 2015).

The water absorption, porosity, bulk density (dry and saturated), and apparent density were performed according to NBR 9778 (ABNT, 2005). For this, the masses of the oven-dry, saturated of surface-dry sample in air and saturated immersed in water test samples were taken in a hydrostatic balance. The water absorption, porosity, bulk density (dry and saturated), and apparent density were calculated according to the following equations.

$$\textit{Water absorption}\ (\%) = \frac{m_{sat} - m_d}{m_d} * 100 \tag{2}$$

$$\textit{Porosity}\ (\%) = \frac{m_{sat} - m_d}{m_{sat} - m_i} * 100 \tag{3}$$

$$\textit{Bulk density, dry}\ \left(\frac{g}{cm^3}\right) = \frac{m_d}{m_{sat} - m_i} * \rho \tag{4}$$

$$\textit{Bulk density, saturated}\ \left(\frac{g}{cm^3}\right) = \frac{m_{sat}}{m_{sat} - m_i} * \rho \tag{5}$$

$$\textit{Apparent density}\ \left(\frac{g}{cm^3}\right) = \frac{m_d}{m_d - m_i} * \rho \tag{6}$$

where m_{sat} is the saturated mass of surface-dry sample in air (g), m_d is the mass of oven-dried sample in air (g), m_i is the saturated mass immersed in water (g) and ρ is the density of water = 1 g/cm^3. For the statistical evaluation of the results of water absorption, porosity, dry bulk density, saturated bulk density and apparent density, the "Anova: Simple Factor" method was used with the aid of Microsoft Excel software and 5% significance level.

The hypothesis checked the ANOVA results of the previous tests cited are similar compared to the control group. For this analysis, a source of variation between groups and within groups was considered. For the P-value test, P values smaller than the significance level reject the equality between the results. Another way of analysing is to compare the value of the critical region (critical F) and the value of F (F). If "F" exceeds the "critical F″ the hypothesis must be rejected.

To evaluate the resistance to acid attack, the 28-day cured specimens were dried in an oven, weighed and submerged in a 5% sulfuric acid solution (v/v) in separate containers. After seven days, the samples were washed, brushed and dried in an oven and weighed again to determine the mass loss. To observe the effect of acid attack on the mortar microstructure, scanning electron microscopy was performed on a Hitachi TM3000 scanning electron microscope under low vacuum with a backscattered electron detector and electron acceleration voltage of 15 kV.

The colourimetric characterisation of the specimens was performed using the CIELab system, in which a polar, cylindrical system represents the colour system. The vertical coordinate (L) represents the degree of brightness of the colour and can assume values between 0 (black) and 100 (white). The coordinates a and b represent the colours and can assume positive or negative values, representing the colours red/green (a/-a), and yellow/blue (b/-b) (López et al., 2016a; Gouveia et al., 2017). The advantage of this system over the RGB (red-green-blue) and CMYK (cyan-magenta-yellow-black) systems is the fact that it might be possible to

Table 1
Composition of cement-based composites with IOT addition.

Composite	Replacement (%)	Mass (g)				w/b
		Portland-cement clinker (~95 wt%) and calcium sulfate (~5 wt%)	IOT	Standard sand	Water	
Control	0	624	0	1872	300	0.48
WHT (without heat treatment and ground)	10	561.6	62.4	1872	300	0.48
	20	499.2	124.8	1872	300	0.48
	30	436.8	187.2	1872	300	0.48
HT 500 (with heat treatment at 500 °C and ground)	10	561.6	62.4	1872	300	0.48
	20	499.2	124.8	1872	300	0.48
	30	436.8	187.2	1872	300	0.48
HT 750 (with heat treatment at 750 °C and ground)	10	561.6	62.4	1872	300	0.48
	20	499.2	124.8	1872	300	0.48
	30	436.8	187.2	1872	300	0.48

numerically calculate the difference of different colours based on the parameters L, a and b (Takatsui et al., 2012). With the aid of Adobe Photoshop software, the variables L, a and b can be easily quantified. For this, nine colour samples were collected in each specimen, being taken the average of the nine measurements.

3. Results and discussion

3.1. IOT characterisation

The results of the chemical analysis are shown in Table 2. The IOT sample is composed of aluminium, silicon and iron oxides, representing 93% by weight, satisfying ASTM C618 and Brazilian Standard NBR 12653 which indicates that the sum of these three oxides must be greater than 50% or 70% depending on the type of pozzolan (ASTM, 2019; ABNT, 2014b). Particular attention should be given to 67% iron oxide, because inorganic pigments are composed of iron oxides, especially red oxides, IOT has great potential as a pigment.

The results of the particle size, pozzolanic activity index, and electrical conductivity are shown in Table 3. All the IOT samples present smaller particle sizes than cement and with 90% of the particles smaller than 36.31 μm for WHT, 27.67 μm for HT500 and 35.79 μm for HT750. The sieve analysis showed that the samples satisfy the ASTM C618 fineness criterion for coal fly ash and raw or calcined natural pozzolan, with less than 34% of the material retained on a 0.045 mm or 45 μm sieve (ASTM, 2019). In the same regard, Brazilian Standard NBR 12653 prescribes that the material to be pozzolanic must be presented with less than 20% of the material retained on a 0.045 mm sieve (ABNT, 2014b). Grain size is an important variable in the evaluation of additive materials in Portland cement (PC), and the smaller particles fill the pores in the cement paste, improving the physical properties through the filler effect (Khan et al., 2017).

In Table 3, it is also shown the pozzolanic activity index (I%) of IOT without and with heat treatment. Generally, it is measured in terms of strength activity index with Portland cement as per ASTM C311 (ASTM, 2018). According to ASTM C618 (ASTM, 2019), the minimum strength activity index with Portland cement should be 75%, as per Brazilian standard NBR 12653 (ABNT, 2014b), the Pozzolanic Activity Index should be at least 90% (Yadav et al., 2019). Analysing the results produced using the method provided by the Brazilian Standard NBR 5752 (ABNT, 2014a), according to the Brazilian Standard NBR 12653 (ABNT, 2014b) only the IOT HT750 showed pozzolanic activity. However, the samples IOT WHT and IOT HT500 obtained pozzolanic activity index results very close to reaching the established minimum and may be characterised as pozzolans.

An important property to consider in materials to be added to Portland cement is the pozzolanic activity. According to Villar-Cociña et al. (2019), many experimental methodologies allow a qualitative or quantitative determination of pozzolanic activity (ASTM, 2018; BS EN, 2005). Several pozzolanic tests have been developed and used by researchers. These include the Chapelle test, the Frattini test, the saturated lime test, and the electrical conductivity measurement (Ramanathan et al., 2019). The last method cited is the method proposed by Luxán et al. (1989), which measures the variation in the electrical conductivity in a saturated calcium hydroxide solution. The measurement of electrical conductivity variation was used to evaluate the pozzolanicity of rice husk ash (Lara and Cordeiro, 2019; Nalobile et al., 2019; Katare and Madurwar, 2020; Vieira et al., 2020), sugarcane bagasse ash (Andreão et al., 2019; Katare and Madurwar, 2019; Rodier et al., 2019; De Soares et al., 2016; Soares et al., 2014), bamboo leaf ash (Rodier et al., 2019), sewage sludge ash (De Azevedo Basto et al., 2019), silica fume (De Soares et al., 2016), waste glass (Alvarenga et al., 2019), clayey soils (Mozejko and Francisca, 2020), spent bleaching earth (Nalobile et al., 2019) and broken bricks (Nalobile et al., 2019).

According to the obtained conductivity variation values (Table 3), the tailings without heat treatment have variable pozzolanicity, while the calcined tailings have good pozzolanicity. The IOT WHT presented a variation of the electrical conductivity (ΔC) in saturated calcium hydroxide solution after 2 min between 0.4 and 1.2 mS cm^{-1}, indicating variable pozzolanicity. Nevertheless, IOT HT500 and IOT HT750 were classified with good pozzolanicity since the mean values of electrical conductivity variation after 2 min was higher than 1.2 mS cm^{-1} for the samples. As results obtained by the same method were also found for other pozzolans (Vieira et al., 2020; Katare and Madurwar, 2020). Also according to Katare and Madurwar (2020), the electrical conductivity pozzolanicity results were consistent with the results of pozzolanic activity index, Chapelle activity, and the amount of reactive silica, which indicates the use of the method proposed by Luxán et al. (1989) for the determination of pozzolanicity.

Thus, in both tests to determine pozzolanicity, the IOT with and without heat treatment presented with pozzolan or very close to being pozzolan. This is because of iron ore tailings exhibit pozzolanic activity after mechanical activation (Yao et al., 2019a, 2020). This behaviour also occurs for other types of tailings, such as gold tailings (Yao et al., 2019b). With the heat treatment, this result was optimized, mainly for the treatment temperature at 750 °C. The IOT 750 presented pozzolanicity in the two tests performed, and this is due to the synergy of the grinding with the heat treatment.

The hues of the samples with and without thermal treatment are shown in Fig. 1. It is possible to notice that the heat treatment

Table 2
Chemical characterisation of reference Portland cement (PC) and iron ore tailings (IOT).

Chemical composition by XRF (wt%)	Portland-cement clinker (~95 wt%) and calcium sulfate (~5 wt%)	IOT
SiO_2	5.10	23.00
Al_2O_3	–	3.20
Fe_2O_3	4.90	66.98
CaO	83.70	–
MgO	–	–
TiO_2	0.30	–
Na_2O	0.10	–
K_2O	0.90	
MnO_2	–	0.56
P_2O_5	–	0.22
Loss on ignition	3.80	6.30
$SiO_2 + Al_2O_3 + Fe_2O_3$ (%)	–	93.18

Table 3
Physical characterisation of reference Portland cement (PC) and iron ore tailings (IOT).

	Portland-cement clinker (~95 wt%) and calcium sulfate (~5 wt%)	IOT		
Particle size distribution		WHT	HT500	HT750
D_M (μm)	18.88	12.26	9.89	16.23
D_{10} (μm)	3.04	0.86	0.87	3.18
D_{50} (μm)	15.92	5.39	5.04	12.51
D_{90} (μm)	39.21	36.31	27.67	35.79
Pozzolanic activity index – I (%)	–	87.8	87.7	90.5
ΔC (mS.cm-1)	–	1.02	1.44	1.68

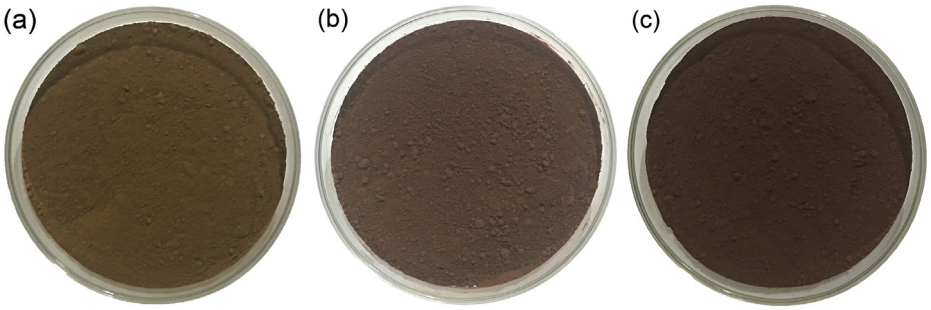

Fig. 1. (a) WHT, (b) HT500 and (c) HT750.

modified the IOT colouration. Such an effect can be explained by the determination of the present phases presented in the diffractogram (Fig. 2). Small clumps are present due to agglomeration of the finer particles.

In Fig. 2 it is shown the diffractograms of the IOT WHT, HT 500 and HT 750 samples. Mineralogical phases of quartz (COD9013321), hematite (COD9015964), goethite (COD1008766) and kaolinite (COD9009234) are identified. Goethite is the mineral specie responsible for the yellow colouration of the IOT WHT sample. In the diffractogram of the IOT HT 500 and HT 750 samples, the goethite peaks are no longer visible because at temperatures above 300 °C (Gialanella et al., 2010; Sikalidis et al., 2006), goethite transforms into hematite, and this mineralogical phase change is responsible for the red hue of the IOT sample after calcination. The peaks corresponding to kaolinite are absent in the diffractogram of the IOT HT 750 sample. This fact is associated with the dehydroxylation of kaolinite during the transformation into metakaolinite, a process that occurs at higher temperatures in the range of 550–700 °C (Boonjaeng et al., 2014; Scrivener et al., 2018).

The thermogravimetric analyses of the IOT WHT, HT 500 and HT

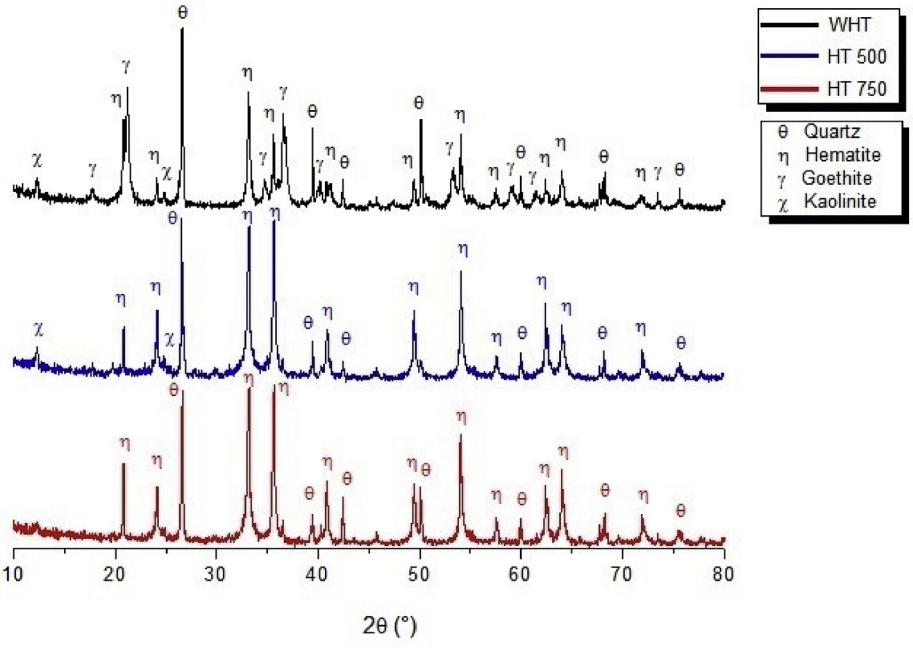

Fig. 2. Diffractograms of the IOT samples.

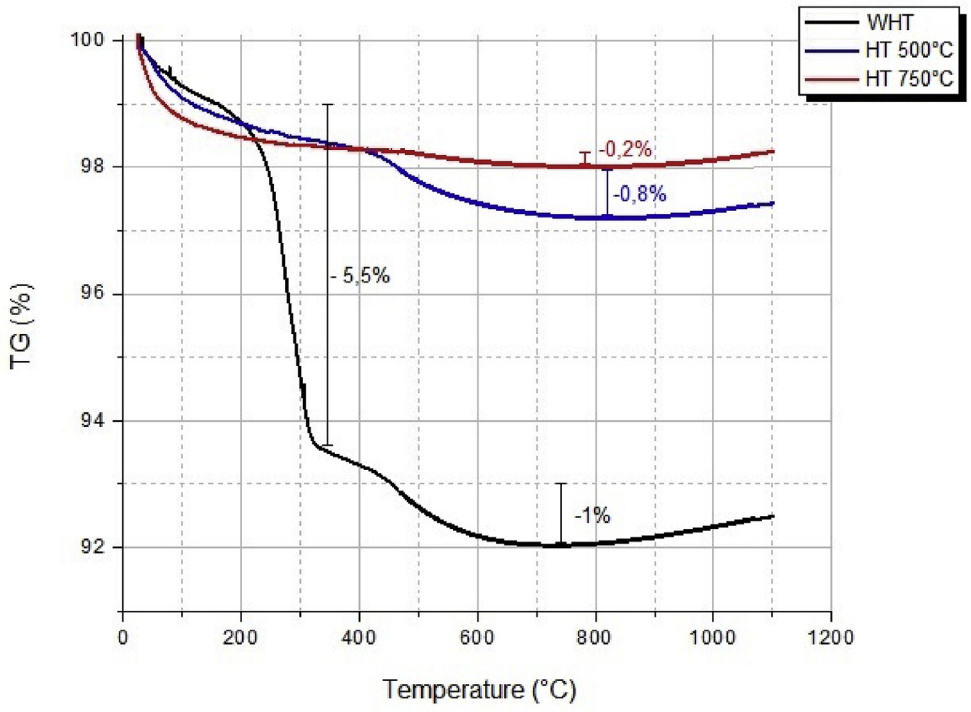

Fig. 3. Thermogravimetric analysis of IOT samples.

750 samples were performed under the same conditions. In Fig. 3 it is possible to compare the results of the three samples; there is no significant mass loss in the 200–300 °C range for the samples that underwent thermal treatment, confirming the transformation of goethite into hematite (Gialanella et al., 2010). A small mass loss occurs above 700 °C that is associated with the dehydroxylation of the kaolinite present in the samples. Compared with the results of the IOT WHT, the IOT HT 500 presents a mass loss of approximately 0.8%, indicating that a large part of the kaolinite present is affected by the thermal treatment. Concerning IOT HT 750, a mass loss of only 0.2% occurs, indicating that most of the kaolinite present in this sample is already in the form of metakaolinite (Boonjaeng et al., 2014; Scrivener et al., 2018). It is worth noting that the results obtained for IOT without heat treatment before and after grinding were the same.

3.2. Physical and mechanical properties of blended cement

In Table 4 it is summarized all the compressive strength results. The main values represent the average of five specimens. The respective standard deviation is expressed in parentheses, the percentage of maintenance of strength as a function of the result of the Control (Reference Portland cement) is shown within brackets and the gain in compressive strength in relation to the previous age is shown within braces.

The compressive strength of the cement with IOT decreases as the incorporation of this waste increases. Values close to the compressive strength of the cement without IOT - Control (Reference Portland cement) - are obtained for incorporations of 10% IOT. The cement with the incorporation of IOT HT 500 and HT 750 show greater gains in compressive strength compared with that of IOT WHT. This gain may be related to the pozzolanic reaction due to the presence of metakaolinite (Scrivener et al., 2018), as the kaolinite peaks of the IOT with thermal treatment disappear in the X-ray diffractograms, also proven by small mass loss occurred above 700 °C which is associated with the dehydroxylation of the kaolinite present in the samples, according to thermogravimetric analysis results. Another fact that explains this behaviour was presented by Yao et al. (2019a), the development of compressive strength indicates that the mechanical ground IOTs exhibit gelling properties in the alkaline environment provided by calcium oxide.

At 28 days, the cement with 10% IOT presented compressive strengths above 40 MPa, meeting the specifications of Portland cement composed with pozzolan – strength class 40 (ABNT, 2018). At 28 days, the cement with 20 and 30% IOT present compressive strengths above 32 MPa, meeting the specifications of pozzolanic Portland cement, according to Brazilian Standard NBR16697 (ABNT, 2018). The compressive strength values obtained for the cement with 30% replacement are higher than those stipulated in the international standard ASTM C1157 for various types of cement, including GU – hydraulic cement for construction (28 MPa) – and RS – high sulfate resistance cement (25 MPa) (ASTM, 2017). As for the 27 products in the family of common cements provided for in EN 197-1 (EN, 2000), Portland cement composed with IOT WHT 10% and 20% can be classified as CEM II/AP and Portland cement composed with IOT WHT 30% can be classified as CEM II/BP. Portland cement composed with IOT HT500 and IOT HT750 10% and 20% can be classified as CEM II/A-Q and Portland cement composed with IOT HT500 and IOT HT750 30% can be classified as CEM II/B-Q. Or they can even be classified as CEM IV/A and CEM IV/B.

Assessing the results of cement with IOT with and without heat treatment at 91 days, all cement showed a gain in compressive strength compared to 28 days. However, the percentage of maintenance of strength as a function of the result of the Control is less than 91 days than at other ages. But, considering the gain in compressive strength in relation to the previous age, the Control was the one that presented the greatest gain at the age of 91 days. This may have been the reason of maintenance of strength as a function of the result of the Control for cements with IOT to have been smaller at this age.

Table 4
Compressive strength for the different cement compositions.

Addition	Replacement (%)	Compressive strength (MPa)			
		3 days	7 days	28 days	91 days
Control	0	32.20[a] (0.75)[b] [100][c] _	41.60 (0.49) [100] {29}[d]	52.30 (1.03) [100] {26}	60.78 (2.76) [100] {16}
WHT	10	29.30 (1.32) [91] _	37.70 (0.36) [91] {29}	48.20 (1.53) [92] {28}	52.45 (2.25) [86] {9}
	20	24.50 (0.86) [76] _	36.30 (1.53) [87] {48}	41.60 (0.92) [80] {15}	42.93 (1.42) [71] {3}
	30	19.70 (0.68) [61] _	31.70 (0.46) [76] {61}	34.00 (1.33) [65] {7}	37.10 (0.80) [61] {9}
HT 500	10	29.60 (1.25) [92] _	38.00 (0.27) [91] {28}	49.40 (1.58) [94] {30}	52.99 (1.37) [87] {7}
	20	25.00 (0.70) [78] _	36.80 (0.80) [88] {47}	42.10 (1.20) [80] {14}	43.80 (1.75) [72] {4}
	30	20.20 (0.57) [63] _	31.30 (0.57) [75] {55}	34.80 (1.35) [67] {11}	38.01 (0.99) [63] {9}
HT 750	10	29.70 (1.19) [92] _	38.90 (0.52) [94] {31}	50.20 (1.19) [96] {29}	54.11 (1.31) [89] {8}
	20	24.90 (1.06) [77] _	37.90 (1.41) [91] {52}	43.40 (1.45) [83] {15}	44.55 (1.68) [73] {3}
	30	20.70 (0.61) [64] _	31.90 (1.45) [77] {54}	35.50 (0.50) [68] {11}	37.21 (1.11) [61] {5}

[a] Compressive strength (MPa).
[b] Standard deviation (MPa).
[c] Maintenance of strength as a function of the result of the Control (%).
[d] Gain in compressive strength in relation to the previous age (%).

Table 5
Flow, water absorption, porosity, bulk density, and apparent density for the different cement compositions.

Addition	Replacement (%)	Flow (mm)	Water absorption (%)	Porosity (%)
Control	0	155	7.98[a] (0.08)[b] [100][c]	16.90 (0.20) [100]
WHT	10	150	8.35 (0.08) [105]	17.36 (0.17) [103]
	20	146	8.10 (0.05) [102]	17.22 (0.07) [102]
	30	145	8.15 (0.03) [102]	16.96 (0.06) [100]
HT 500	10	151	8.35 (0.08) [105]	17.46 (0.15) [103]
	20	150	8.35 (0.16) [105]	17.80 (0.20) [105]
	30	146	8.28 (0.15) [104]	17.27 (0.22) [102]
HT 750	10	168	8.31 (0.13) [104]	17.23 (0.44) [102]
	20	150	8.12 (0.09) [102]	17.31 (0.12) [102]
	30	146	8.03 (0.03) [101]	16.78 (0.09) [99]

[a] Average of three specimens.
[b] Standard deviation.
[c] Maintenance of properties displayed as a function of the result of the Control (%).

The standard deviation found for the results were low and within the limit provided by Brazilian standard NBR 7215 (ABNT, 2019). It is worth mentioning the relationship between the compressive strength results of the cement produced with IOT and tested according to the Brazilian standard NBR 7215 (ABNT, 2019) and the strength activity index with Portland cement predicted for ASTM C311 (ASTM, 2018).

As previously mentioned, the Brazilian standard NBR 7215 prescribes the production of mortar with binder/aggregate ratio equal to 3 and water/cement ratio equal to 0.48 for the evaluation of Portland cement compressive strength (ABNT, 2019). ASTM C311 prescribes the production of two mortars with binder/aggregate ratio equal to 2.75 and water/cement ratio equal to 0.484. It follows that the second mortar will be replaced by 20% of Portland cement with the material to be evaluated as pozzolan, and a water/cement ratio varied as a function of the amount of water required for flow ±5 of the control mixture (ASTM, 2018).

Despite the differences in the cited standards, Brazilian standard NBR 7215 and ASTM (ABNT, 2019; ASTM, 2018), some analysis can be performed with caveats. Considering that the present work produced Portland cements with 10%, 20% and 30% of IOT with and without heat treatment and evaluated the compressive strength of cement produced according to the Brazilian standard NBR 7215, the results of compressive strength for cements with 20% IOT can somehow be compared with the strength activity index with Portland cement calculated according to ASTM C311 (ASTM, 2018). Of course, differences in binder/aggregate and water/cement ratios may affect the properties of the mortars produced. However, differences in binder/aggregate and water/cement ratios occur simultaneously for control mortar and IOT mortars within the results presented, because it is a comparative analysis. So, the authors believe that the percentage of maintenance of strength as a function of the result of the Control (Reference Portland cement). This value is shown within brackets (Table 4) for mixtures with 20% IOT and can be compared with the strength activity index with Portland cement. Since, as ASTM C618 (ASTM, 2019) provides for the assessment of the strength activity index with Portland cement at 7 and 28 days, under these considerations and caveats, mortars produced with cement with 20% IOT with and without treatment performed satisfactorily, as they presented the percentage of maintenance of strength as a function of the result of the Control (Reference Portland cement) higher than the 75% strength activity index with Portland cement predicted by ASTM. C618 (ASTM, 2019).

In Tables 5 and 6 it is possible to observe the results of the water absorption, porosity, bulk density, and apparent density tests performed at 28 days of curing, along with the flow. The main values represented the average of three specimens and the respective

Table 6
Bulk density and apparent density for the different cement compositions.

Addition	Replacement (%)	Bulk density, dry (g/cm^3)	Bulk density, saturated (g/cm^3)	Apparent density (g/cm^3)
Control	0	2.117	2.286	2.547
		(0.003)	(0.005)	(0.010)
		[100]	[100]	[100]
WHT	10	2.080	2.254	2.517
		(0.005)	(0.005)	(0.008)
		[98]	[99]	[99]
	20	2.125	2.297	2.567
		(0.005)	(0.005)	(0.004)
		[100]	[100]	[101]
	30	2.080	2.250	2.505
		(0.005)	(0.006)	(0.008)
		[98]	[98]	[98]
HT 500	10	2.091	2.266	2.533
		(0.002)	(0.001)	(0.002)
		[99]	[99]	[99]
	20	2.132	2.310	2.594
		(0.016)	(0.014)	(0.013)
		[101]	[101]	[102]
	30	2.086	2.259	2.522
		(0.011)	(0.010)	(0.009)
		[99]	[99]	[99]
HT 750	10	2.073	2.245	2.505
		(0.023)	(0.027)	(0.040)
		[98]	[98]	[98]
	20	2.131	2.304	2.577
		(0.012)	(0.011)	(0.012)
		[101]	[101]	[101]
	30	2.089	2.257	2.510
		(0.003)	(0.004)	(0.006)
		[99]	[99]	[99]

[a] average of three specimens; [b] standard deviation; [c] maintenance of properties displayed as a function of the result of the Control (%).

standard deviation is expressed in parentheses and the percentage of maintenance of properties displayed as a function of the result of the Control (Reference Portland cement) is shown within brackets.

The amount of absorbed water in the mortars produced with the cement with IOT slightly increases, and the same it occurs with the porosity. Despite the fine particle size of the IOT, which leads to a loss of workability, these particles occupy the macro and micro-pores formed during cement hydration and contributed to a decrease in the porosity of the mortar (Shettima et al., 2016; Yaprak et al., 2011). Porosity is a factor directly related to the durability of concrete and mortars regarding the attack by acidic substances. The higher the porosity and permeability are the higher the rate of percolation of substances and the greater the degradation suffered by the concrete or mortar (Kim et al., 2014). However, the addition of IOT to slightly increased porosity contributes negatively to durability. The consistency index of the mortars with additions does not significantly vary despite the IOT being finer and increasing the amount of water or using a plasticiser additive was not necessary.

Bulk density and apparent density for HT500 and HT750 were slightly higher than WHT. This suggests that the heat treatment of the IOT can influence these properties.

As can be seen in Table 7, the results of water absorption are considered similar to the control group at specimens with 500 °C of heat treatment. In the specimens without heat treatment, the P-value is smaller than the significance level (0,05) and the critical F is bigger than the value of F. So in this case, the calcination directly influences this parameter, since the heat treatment promotes the dehydroxylation of kaolinite in metakaolin and the reaction of silica presented in metakaolin favours the formation of cement hydration products and consequently decreases the material's water absorption (Mojekzo and Francisca, 2020). With 750 °C of heat treatment, the results are considered not similar with the control group. However, the sum of the squares (SQ) between the groups is smaller; that is, there is a smaller variation in relation to the average than in the case without heat treatment. In the porosity tests, similar behaviour can be observed. In this test, only the specimens with 750 °C are considered equal to the group control. For dry bulk density, saturated bulk density and apparent density, the results are not considered similar on the statistical evaluation. The specimens without heat treatment presented smaller P-values than the specimens whit heat treatment for all the tests. This suggests that

Table 7
Statistical analysis of physical properties.

Physical property	Heat treatment	SQ[a]	F-ratio[b]	p-value
Water absorption	WHT	0,17660	14,42177	0,00221
	500 HT	0,19985	4,15175	0,05515
	750 HT	0,16647	6,53511	0,01939
Porosity	WHT	0,38465	7,46190	0,01386
	500 HT	1,03367	9,03783	0,00835
	750 HT	0,56178	2,71986	0,12445
Dry bulk density	WHT	0,00475	65,26047	0,00002
	500 HT	0,00417	12,57516	0,00331
	750 HT	0,00602	10,64747	0,00532
Saturated bulk density	WHT	0,00469	57,98495	0,00003
	500 HT	0,00478	19,01923	0,00096
	750 HT	0,00637	8,51371	0,00980
Apparent density	WHT	0,00693	42,07358	0,00008
	500 HT	0,00906	35,79112	0,00013
	750 HT	0,01034	6,480535	0,01980

Notes.
[a] SQ = Sun squares.
[b] $F_{critical} = 4{,}34683$.

the heat treatment influences on these properties of the material.

3.3. Coulorimetric characterisation of blended cements

Fig. 4(a)-(c) presents the test specimens of the cement with IOT WHT, IOT HT 500 and HT 750, respectively, with the cement without IOT on the left and the replacement percentages increasing from left to right. As shown in Fig. 4, higher replacement percentages provide stronger hues.

The colour codes obtained via the image analysis CIELab are shown in Table 8. The colour analysis using the CIELab system shows that the parameters a and b of the control specimen presented lower values than the others. The smaller modulus of these parameters and the closer to the vertical axis, the colour assumes shades of grey ranging from white to black. The specimens composed by IOT without heat treatment presented variable values of b and this parameter is higher than other specimens, tending to yellow due to the presence of goethite.

After heat treatment, goethite is converted to hematite, resulting in higher variable values for the specimens, tending to red. As for the parameter L, the specimens with IOT are smaller and, therefore, darker than the control specimen. The lack of a standard for this variable may reflect the poor homogenisation of the mortar or segregation during its conformation (López et al., 2016a, 2016b). Galvão et al. (2018) suggested that the iron ore tailings can be used as pigment for sustainable paints. So, the various colours found in the colourimetric characterisation due to the calcination is advantageous from the aesthetic aspect.

Table 8
Colour codes of the specimens.

Addition	Replacement (%)	CIELab system		
		L	a	b
Control	0	61,3	−2	8
WHT	10	52,6	2,9	24,3
	20	42,4	8,0	27,4
	30	45,2	12,0	29,7
HT500	10	49,6	11,7	22,0
	20	34,3	13,2	19,8
	30	40,0	15,0	19,9
HT750	10	43,0	8,2	14,8
	20	41,4	13,1	17,4
	30	36,9	12,8	14,8

Table 9
Mass loss values after acid attack.

Addition	Replacement (%)	Mass loss (%)
Control	0	19.8
WHT	10	17.8
	20	15.0
	30	13.0
HT 500	10	17.7
	20	14.6
	30	12.3
HT 750	10	17.1
	20	13.2
	30	11.8

3.4. Resistance to acid attack of blended cements

In Table 9 it is possible to observe that the mass loss values of the mortars produced with the different types of cement after attack by sulfuric acid solution. This acid was chosen because of its high acidity, being extremely aggressive to cementitious compounds.

The use of sulfuric acid for mortar degradation has been evaluated in other studies, including Živica (2004) and Gutberlet et al. (2015). Resistance to attack is related to the pore size distribution (Zivica and Bajza, 2001) in addition to the cement chemistry and aggregates involved. According to the results obtained in the water absorption tests, the mortars produced with the cement with IOT incorporated have slightly higher porosity and therefore, a higher amount of attack are expected in these samples. However, the mass

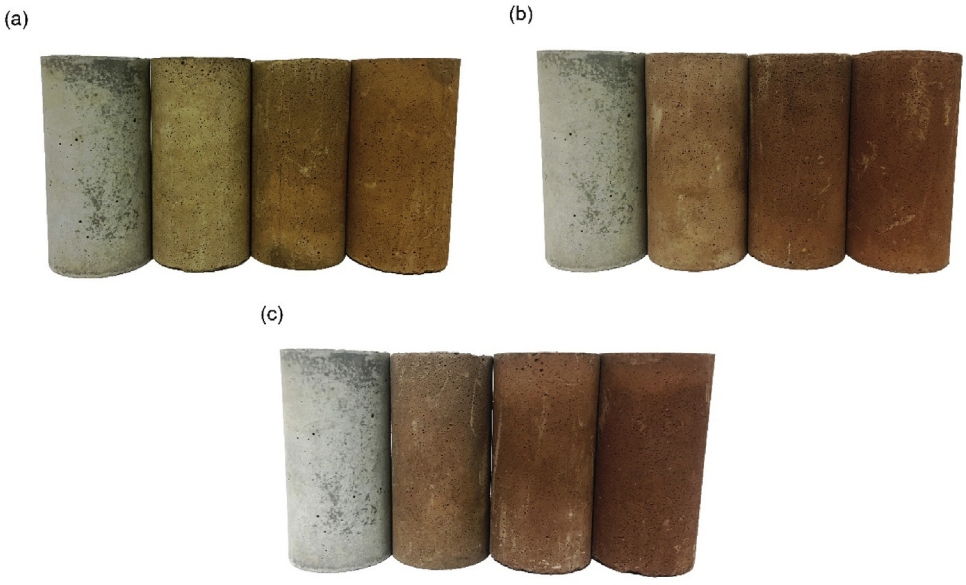

Fig. 4. Test specimens produced with the cement developed.

loss is lower in the samples produced with cement with IOT incorporated, decreasing with increasing incorporation percentage. The calcium hydroxide generated by the hydration of the Portland cement is the component with the lowest chemical stability and is highly vulnerable to acidic substances. Because the cement without IOT contains a greater amount of Portland clinker, this cement generates a greater amount of $Ca(OH)_2$. In the reaction between sulfuric acid and $Ca(OH)_2$, gypsum ($CaSO_4.2H_2O$) is formed, which in turn reacts with the calcium aluminate in the matrix and forms ettringite ($3CaO.Al_2O_3.3CaSO_4.31H_2O$) (Zivica and Bajza, 2002). Gypsum and ettringite are expansive products that increase the porosity and the surface permeability, accelerating the rate of attack by acidic substances. Thus, the addition of IOT reduces the amount of generated $Ca(OH)_2$ and reduces the vulnerability of the concrete to acid attack (Gutberlet et al., 2015). For the same percentage of incorporation, the mass loss decreases as the IOT thermal treatment temperature increases. The pozzolanic reaction of the metakaolinite presented in IOT consumed part of the $Ca(OH)_2$ generated during the hydration and decreased the availability of $Ca(OH)_2$ to react with sulfuric acid.

In Fig. 5 it is possible to observe the IOT WHT (Fig. 5(a)), HT 500 (Fig. 5(b)) and HT 750 (Fig. 5(c)) cement test specimens after acid attack. Variation in the intensity of the acid attack in the specimens produced with the cement without IOT is noticeable, and with increasing the proportion of IOT, the acid wear is less intense. The surface integrity of pastes was deteriorated as an increase in mass loss and surface roughness was found when compared to the initial state before sulfuric acid attack. Although all samples in contact with sulfuric acid exhibit increased surface roughness and aggregate exposure, these effects are greatly minimised in IOT samples, with partially intact areas in the specimens with 30% IOT, especially in the 30% IOT HT750 sample.

To illustrate the effect of the acid attack on the microstructure, micrographs obtained from the cement specimens without IOT (Fig. 6(a)) and cement with 30% IOT (Fig. 6(b)) are shown in Fig. 6, as these specimens have the highest and lowest mass loss values, respectively. Acicular structures were formed in both compositions. Because sulfuric acid releases sulfate ions when in solution, it is believed that this structure is ettringite. Monosulfoaluminate derived from the presence of tricalcium aluminate (C_3A) in Portland cement in sulfate and sulfuric acid attack forms an expansive secondary ettringite that causes internal damages to the material structure (Khan et al., 2019). In the cement without IOT (Fig. 6(a)), the matrix is spongy and rough, showing the high apparent porosity, the removal of a large part of the original surface, the formation of cracks, and with large gypsum and ettringite crystals, as also found in Portland cement concrete after sulfuric acid attack (Gu et al., 2019). In the cement matrix with 30% IOT (Fig. 6(b)), despite the presence of ettringite, the matrix is still cohesive, with lower apparent porosity and no large removal of unconsolidated surface material. Most likely, the greatest resistance to attack was provided by the pozzolanic reaction and the change in the $(SiO_2 + Al_2O_3 + Fe_2O_3)/CaO$ ratio (Lara and Cordeiro, 2019). Grandclerc et al. (2018) point out that the addition of blast furnace slag, pozzolans, and fly ashes reduces the production of gypsum and ettringite when the cement is under attack by sulfuric acid.

4. Conclusions

Based on experiments and theoretical analysis, the following can be concluded:

(1) The IOT presented chemical composition and particle size that meet Brazilian and international standards to be considered a pozzolanic material.
(2) The IOT with and without heat treatment showed variable pozzolanicity and good pozzolanicity according to the electrical conductivity. The IOT HT750 presented a pozzolanic activity index that characterises it as a pozzolan according to the Brazilian standard. The IOT WHT and HT500 obtained

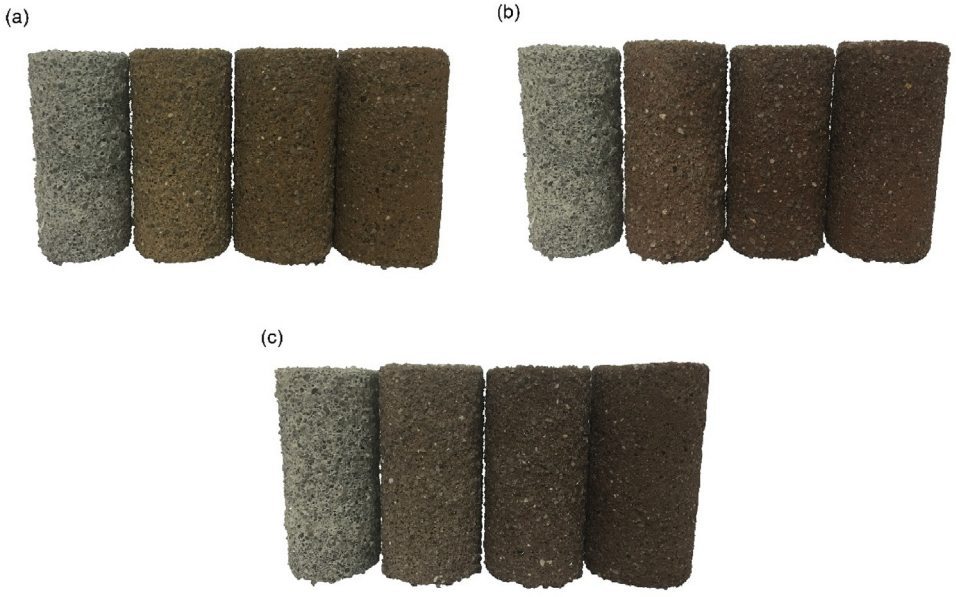

(a) IOT 10% after sulphuric acid attack; (b) IOT 20% after sulphuric acid attack; and (c) IOT 30% after sulphuric acid attack.

Fig. 5. Test specimens after acid attack.

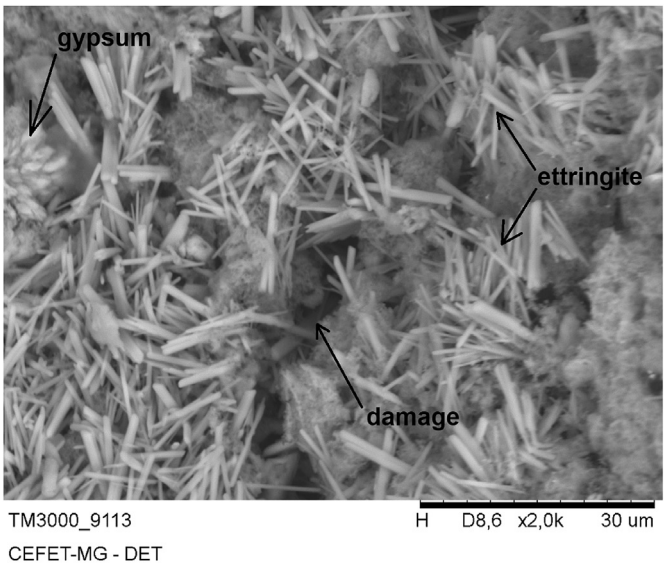

(a)

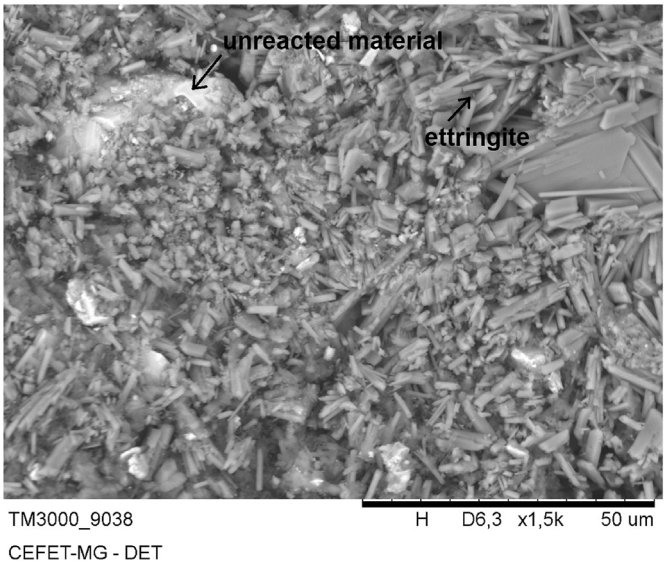

(b)

Fig. 6. Microscope images of the test specimens produced with (a) cement without IOT and (b) cement with 30% IOT after acid attack.

indexes close to being characterised as pozzolan. As a result, heat treatment at 750 °C leads to better pozzolanicity.

(3) The kaolinite from the IOT is extinguished by heat treatment at 750 °C, a fact confirmed by X-ray diffraction and thermogravimetric analysis.

(4) The mechanical strength of IOT composite cements was compatible with Brazilian and international standards. Also, the compressive strength values established in Portland cement standards have been met with a 30% reduction in clinker consumption, which can reduce CO_2 emissions.

(5) IOT compound cement were more durable under severe acid attack. The presence of IOT inhibited the formation of harmful phases and increased durability.

(6) The heat-treated IOT produced cement with different matrices, creating the opportunity to produce cement in colours other than grey or white. This option can be interesting for use in structures that will be seen by the public and will eliminate the need for subsequent coloured coating layers, such as mortars and paints.

(7) The physical parameters (water absorption, porosity, bulk density, and apparent density) of mortars produced with IOT composite cement were compatible with the mortar produced with the reference Portland cement.

(8) The encapsulation of IOT by cement as SCM represents a viable option for immobilising large volumes of this mining waste, reducing the impacts of tailings dams.

(9) The synergy of the IOT grinding and heat treatment led to a better composite cement within the studied parameters. The results showed that the partial replacement of clinker by IOT in the production of composite cement is effective for use on a large scale, consumes less energy because the calcination temperature of the IOT is lower than the sintering temperature of the clinker and is ecologically correct when adding value to IOT, generating a differentiated product with different colours.

Funding

This work was supported by the Minas Gerais State Research Foundation (FAPEMIG) [grant numbers APQ-03739-16, APQ-00368-17]; and the Brazilian Federal Agency for Support and Evaluation of Graduate Education (CAPES) [grant number 001].

Role of the funding source

The funding sources were not involved in the work reported in this paper.

CRediT authorship contribution statement

Luciano Fernandes de Magalhães: Conceptualization, Methodology, Software, Investigation, Writing - original draft, Writing - review & editing, Visualization. **Sâmara França:** Investigation, Writing - original draft, Writing - review & editing, Visualization. **Michelly dos Santos Oliveira:** Supervision. **Ricardo André Fiorotti Peixoto:** Writing - original draft. **Sofia Araújo Lima Bessa:** Data curation, Supervision, Writing - original draft, Writing - review & editing. **Augusto Cesar da Silva Bezerra:** Validation, Resources, Data curation, Writing - original draft, Writing - review & editing, Supervision, Project administration, Funding acquisition.

Declaration of competing interest

The authors declare that they have no known competing financial interests or personal relationships that could have appeared to influence the work reported in this paper.

Acknowledgements

The authors would like to express their gratitude to Minas Gerais State Research Foundation (FAPEMIG APQ3739-16), to the Brazilian Federal Agency for Support and Evaluation of Graduate Education (Coordenação de Aperfeiçoamento de Pessoal de Nível Superior - CAPES) for their financial support in scientific initiation and master's degree scholarships (Finance Code 001).

References

ABNT, 2005. NBR 9778: Argamassa e Concreto Endurecidos: Determinação da

Absorção de Água por Imersão — Índice de Vazios e Massa Específica. Associação Brasileira de Normas Técnicas, Rio de Janeiro.
ABNT, 2014a. NBR 5752: Materiais pozolânicos - determinação do índice de desempenho com cimento portland aos 28 dias. Associação Brasileira de Normas Técnicas, Rio de Janeiro.
ABNT, 2014b. NBR 12653: Materiais Pozolânicos - Requisitos. Associação Brasileira de Normas Técnicas, Rio de Janeiro.
ABNT, 2015. NBR 7214: Areia Normal para Ensaio de Cimento - Especificação. Associação Brasileira de Normas Técnicas, Rio de Janeiro.
ABNT, 2018. NBR 16697: Cimento Portland - Requisitos. Associação Brasileira de Normas Técnicas, Rio de Janeiro.
ABNT, 2019. NBR 7215: Cimento Portland - Determinação da Resistência à Compressão. Associação Brasileira de Normas Técnicas, Rio de Janeiro.
Aires, U.R.V., Santos, B.S.M., Coelho, C.D., Da Silva, D.D., Calijuri, M.L., 2018. Changes in land use and land cover as a result of the failure of a mining tailings dam in Mariana, MG, Brazil. Land Use Pol. 70, 63–70. https://doi.org/10.1016/j.landusepol.2017.10.026.
Alvarenga, C.B.C.S., Heiderick, O.M., Couto, T.A., Cetlin, P.R., Sales, R.B.C., Aguilar, M.T.P., 2019. Influence of soda-lime waste glass microparticles on workability and thermal properties of portland cement compounds. Mater. Construcción 69 (335), e192. https://doi.org/10.3989/mc.2019.05818.
Amran, Y.H. Mugahed, Alyousef, Rayed, Alabduljabbar, Hisham, El-Zeadani, Mohamed, 2020. Clean production and properties of geopolymer concrete; A review. J. Clean. Prod. 251, 119679. https://doi.org/10.1016/j.jclepro.2019.119679.
Andreão, P.V., Suleiman, A.R., Cordeiro, G.C., Nehdi, M.L., 2019. Beneficiation of sugarcane bagasse ash: pozzolanic activity and leaching behavior. Waste and Biomass Valorization 1–10. https://doi.org/10.1007/s12649-019-00721-x.
ASTM, 2014. Standard Specification for Flow Table for Use in Tests of Hydraulic Cement. ASTM International, West Conshohocken, Philadelphia, United States of America. ASTM C230/C230M-14.
ASTM, 2015. Standard Test Method for Flow of Hydraulic Cement Mortar. ASTM International, West Conshohocken, Philadelphia, United States of America. ASTM C1437-15.
ASTM, 2017. Standard Performance Specification for Hydraulic Cement. ASTM International, West Conshohocken, Philadelphia, United States of America. ASTM C1157/C1157M-17.
ASTM, 2018. Test Methods for Sampling and Testing Fly Ash or Natural Pozzolans for Use in Portland-Cament Concrete. ASTM International, West Conshohocken, Philadelphia, United States of America. ASTM C311/C311M-18.
ASTM, 2019. Specification for Coal Fly Ash and Raw or Calcined Natural Pozzolan for Use in Concrete. ASTM International, West Conshohocken, Philadelphia, United States of America. ASTM C618-19.
Bastos, L.A.D.C., Silva, G.C., Mendes, J.C., Peixoto, R.A.F., 2016. Using iron ore tailings from tailing dams as road material. J. Mater. Civ. Eng. 28, 04016102 https://doi.org/10.1061/(ASCE)MT.1943-5533.0001613.
Bezerra, A.C.S., Saraiva, S.L.C., Lara, L.F.S., Castro, L.W.A., Gomes, R.C., Rodrigues, C.S., Ferreira, M.C.N., Aguilar, M.T., 2017. Effect of partial replacement with thermally processed sugar cane bagasse on the properties of mortars. Rev. Mater. 22 https://doi.org/10.1590/s1517-707620170001.0117.
Bezerra, A.C.S., França, S., Magalhães, L.F., Carvalho, M.C.R., 2019. Alkaline activation of high-calcium ash and iron ore tailings and their recycling potential in building materials. Ambiente Construído 19, 99–112. https://doi.org/10.1590/s1678-86212019000300327.
Bhagath Singh, G.V.P., Subramaniam, K.V.L., 2019. Production and characterization of low-energy Portland composite cement from post-industrial waste. J. Clean. Prod. 239 https://doi.org/10.1016/j.jclepro.2019.118024.
Boonjaeng, S., Chindaprasirt, P., Pimraksa, K., 2014. Lime-calcined clay materials with alkaline activation: phase development and reaction transition zone. Appl. Clay Sci. 95, 357–364. https://doi.org/10.1016/j.clay.2014.05.002.
BS EN, 2005. British Standard Euronorm 196.: Methods of Testing Cement. Part 5: Pozzolanicity Test for Pozzolanic Cement.
Cavallini, M., 2019. Mina que abriga barragem em Brumadinho responde por 2% da produção da Vale; veja raio-X. https://g1.globo.com/economia/noticia/2019/01/28/mina-que-abriga-barragem-em-brumadinho-responde-por-2-da-producao-da-vale-veja-raio-x.ghtml. (Accessed 18 February 2019).
Chaturvedi, N., Ahmed, M.J., Dhal, N.K., 2014. Effects of iron ore tailings on growth and physiological activities of *Tagetes patula* L. J. Soils Sediments 14, 721–730. https://doi.org/10.1007/s11368-013-0777-0.
Cui, X.W., Wang, C.L., Ni, W., Di, Y.Q., Cui, H.L., Chen, L., 2017. Studiulmecanismului de reactieînbetonulcelularautoclavizat cu continut de deseuri de minereu cu fier/Study on the reaction mechanism of autoclaved aerated concrete based on iron ore tailings. Rev. Română Mater. 47, 46–53.
Davies, M.P., 2002. Tailings impoundment failures: are geotechnical engineers listening. Geotech. News 20, 31–36.
De Azevedo Basto, P., Savastano Junior, H., de Melo Neto, A.A., 2019. Characterization and pozzolanic properties of sewage sludge ashes (SSA) by electrical conductivity. Cement Concr. Compos. 104 https://doi.org/10.1016/j.cemconcomp.2019.103410.
De Soares, M.M.N.S., Garcia, D.C.S., Figueiredo, R.B., Aguilar, M.T.P., Cetlin, P.R., 2016. Comparing the pozzolanic behavior of sugar cane bagasse ash to amorphous and crystalline SiO2. Cement Concr. Compos. 71, 20–25. https://doi.org/10.1016/j.cemconcomp.2016.04.005.
Díaz, Y.C., Sánchez, S., Heierli, U., Favier, A.R., Machado, I.R.S., Scrivener, K.L., Hernández, J.F.M., Habert, G., 2017. Limestone calcined clay cement as a low-carbon solution to meet expanding cement demand in emerging economies. Dev. Eng. 2, 82–91. https://doi.org/10.1016/j.deveng.2017.06.001.
EN (European norm), 2000. EN 197–1, Cement - Part 1: Composition, Specifications and Conformity Criteria for Common Cements, European Standard. European Committee for Standardization.
Fontes, W.C., Fontes, G.G., Costa, E.C.P., Mendes, J.C., Silva, G.J.B., Peixoto, R.A.F., 2018. Iron ore tailings in the production of cement tiles: a value analysis on building sustainability. Ambiente Construído 18, 395–412. https://doi.org/10.1590/s1678-86212018000400312.
Galvão, J.L.B., Andrade, H.D., Brigolini, G.J., Peixoto, R.A.F., Mendes, J.C., 2018. Reuse of iron ore tailings from tailings dams as pigment for sustainable paints. J. Clean. Prod. 200, 412–422. https://doi.org/10.1016/j.jclepro.2018.07.313.
Gerais, Minas, 2019. Sobe para 169 o número de mortos identificados na tragédia da Vale, em Brumadinho. https://g1.globo.com/mg/minas-gerais/noticia/2019/02/17/sobe-para-169-o-numero-de-mortos-identificados-na-tragedia-da-vale-em-brumadinho.ghtml. (Accessed 18 February 2019).
Ghalehnovi, M., Roshan, N., Hakak, E., Shamsabadi, E.A., de Brito, J., 2019. Effect of red mud (bauxite residue) as cement replacement on the properties of self-compacting concrete incorporating various fillers. J. Clean. Prod. 240 https://doi.org/10.1016/j.jclepro.2019.118213.
Gialanella, S., Girardi, F., Ischia, G., Lonardelli, I., Mattarelli, M., Montagna, M., 2010. On the goethite to hematite phase transformation. J. Therm. Anal. Calorim. 102, 867–873. https://doi.org/10.1007/s10973-010-0756-2.
Gouveia, P.F., Schabbach, L.M., Souza, J.C.M., Henriques, B., Labrincha, J.A., Silva, F.S., et al., 2017. New perspectives for recycling dental zirconia waste resulting from CAD/CAM manufacturing process. J. Clean. Prod. 152, 454–463. https://doi.org/10.1016/j.jclepro.2017.03.117.
Grandclerc, A., Dangla, P., Gueguen-Minerbe, M., Chaussadent, T., 2018. Modelling of the sulfuric acid attack on different types of cementitious materials. Cement Concr. Res. 105, 126–133. https://doi.org/10.1016/j.cemconres.2018.01.014.
Gu, L., Bennett, T., Visintin, P., 2019. Sulphuric acid exposure of conventional concrete and alkali-activated concrete: assessment of test methodologies. Construct. Build. Mater. 197, 681–692. https://doi.org/10.1016/j.conbuildmat.2018.11.166.
Guimaraes, N.C., Valadao, G.E.S., Peres, A.E.C., 2012. Filtragem de rejeitos de minério de ferro visando à sua disposição em pilhas. Rev. Esc. Minas 65, 543–548. https://doi.org/10.1590/S0370-44672012000400016.
Gutberlet, T., Hilbig, H., Beddoe, R.E., 2015. Acid attack on hydrated cement — effect of mineral acids on the degradation process. Cement Concr. Res. 74, 35–43. https://doi.org/10.1016/j.cemconres.2015.03.011.
Hospodarova, V., Junak, J., Stevulova, N., 2015. Color pigments in concrete and their properties. Pollack Period. 10, 143–151. https://doi.org/10.1556/606.2015.10.3.15.
Huang, X., Ranade, R., Li, V.C., 2012. Feasibility study of developing green ecc using iron ore tailings powder as cement replacement. J. Mater. Civ. Eng. 25, 923–931. https://doi.org/10.1061/(ASCE)MT.1943-5533.0000674.
Imbabi, M.S., Carrigan, C., McKenna, S., 2012. Trends and developments in green cement and concrete technology. Int. J. Sustain. Built Environ. 1, 194–216. https://doi.org/10.1016/j.ijsbe.2013.05.001.
Jankovský, O., Pavlíková, M., Sedmidubský, D., Bouša, D., Lojka, M., Pokorný, J., et al., 2017. Study on pozzolana activity of wheat straw ash as potential admixture for blended cements. Ceramics 61 (4), 327–339. https://doi.org/10.13168/cs.2017.0032.
Katare, V.D., Madurwar, M.V., 2019. Use of processed biomass ash as a sustainable pozzolana. Curr. Sci. 116, 741–750. https://doi.org/10.18520/cs/v116/i5/741-750.
Katare, V.D., Madurwar, M.V., 2020. Design and investigation of sustainable pozzolanic material. J. Clean. Prod. 242 https://doi.org/10.1016/j.jclepro.2019.118431.
Ke, X., Zhou, X., Wang, X., Wang, T., Hou, H., Zhou, M., 2016. Effect of tailings fineness on the pore structure development of cemented paste backfill. Construct. Build. Mater. 126, 345–350. https://doi.org/10.1016/j.conbuildmat.2016.09.052.
Keppert, M., Urbanová, M., Brus, J., Čáchová, M., Fořt, J., Trník, A., et al., 2017. Rational design of cement composites containing pozzolanic additions. Construct. Build. Mater. 148, 411–418. https://doi.org/10.1016/j.conbuildmat.2017.05.032.
Khan, M.N.N., Jamil, M., Karim, M.R., Zain, M.F.M., Kaish, A.B.M.A., 2017. Filler effect of pozzolanic materials on the strength and microstructure development of mortar. KSCE J. Civil Eng. 21, 274–284. https://doi.org/10.1007/s12205-016-0737-5.
Khan, H.A., Castel, A., Khan, M.S.H., Mahmood, A.H., 2019. Durability of calcium aluminate and sulphate resistant Portland cement based mortars in aggressive sewer environment and sulphuric acid. Cement Concr. Res. 124 https://doi.org/10.1016/j.cemconres.2019.105852.
Kim, Y.-Y., Lee, K.-M., Bang, J.-W., Kwon, S.-J., 2014. Effect of W/C ratio on durability and porosity in cement mortar with constant cement amount. Ann. Mater. Sci. Eng. 2014, 1–11. https://doi.org/10.1155/2014/273460.
Kuranchie, F.A., Shukla, S.K., Habibi, D., Mohyeddin, A., 2015. Utilisation of iron ore tailings as aggregates in concrete. Cogent Eng 2, 1083137. https://doi.org/10.1080/23311916.2015.1083137.
Lacaz, F.A.C., Porto, M.F.S., Pinheiro, T.M.M., 2017. Tragédias brasileiras contemporâneas: o caso do rompimento da barragem de rejeitos de Fundão/Samarco. Rev. Bras. Saúde Ocup. 42 https://doi.org/10.1590/2317-6369000016016.
Lange, C.A., Kotte, K., Smit, M., Van Deventer, P.W., Van Rensburg, L., 2012. Effects of different soil ameliorants on karee trees (*Searsia lancea*) growing on mine

tailings dump soil-part I: pot trials. Int. J. Phytoremediation 14, 908–924. https://doi.org/10.1080/15226514.2011.636402.
Lara, R.C., Cordeiro, G.C., 2019. Effect of rice husk ash as supplementary cementitious material on the performance of cement-based pastes continuously exposed to organic acid solution (vinasse). J. Mater. Civ. Eng. 31 (7) https://doi.org/10.1061/(ASCE)MT.1943-5533.0002739.
Lee, H.-S., Lee, J.-Y., Yu, M.-Y., 2005. Influence of inorganic pigments on the fluidity of cement mortars. Cement Concr. Res. 35, 703–710. https://doi.org/10.1016/j.cemconres.2004.06.010.
Li, X., Park, J.H., Edraki, M., Baumgartl, T., 2014. Understanding the salinity issue of coal mine spoils in the context of salt cycle. Environ. Geochem. Health 36, 453–465. https://doi.org/10.1007/s10653-013-9573-4.
López, A., Guzmán, G.A., Di Sarli, A.R., 2016a. Color stability in mortars and concretes. Part 1: study on architectural mortars. Construct. Build. Mater. 120, 617–622. https://doi.org/10.1016/j.conbuildmat.2016.05.133.
López, A., Guzmán, G.A., Di Sarli, A.R., 2016b. Color stability in mortars and concretes. Part 2: study on architectural concretes. Construct. Build. Mater. 123, 248–253. https://doi.org/10.1016/j.conbuildmat.2016.06.147.
Luxán, M.P., Madruga, F., Saavedra, J., 1989. Rapid evaluation of pozzolanic activity of natural products by conductivity measurement. Cement Concr. Res. 19 (1), 63–68. https://doi.org/10.1016/0008-8846(89)90066-5.
Magalhães, L.F.D., Morais, I.D.S., Lara, L.F.D.S., Resende, D.S.D., Menezes, R.M.R.O., Aguilar, M.T.P., Bezerra, A.C.D.S., 2018. Iron ore tailing as addition to partial replacement of Portland cement. Mater. Sci. Forum 930, 125–130. https://doi.org/10.4028/www.scientific.net/MSF.930.125.
Morais, I.D.S., Magalhães, L.F.D., Lara, L.F.D.S., Corrêa, E.C.S., Menezes, R.M.R.O., Aguilar, M.T.P., Bezerra, A.C.D.S., 2018. Sericitic phyllite as addition in Portland cement. Mater. Sci. Forum 930, 131–136. https://doi.org/10.4028/www.scientific.net/MSF.930.131.
Mouazen, A.M., Alhwaimel, S.A., Kuang, B., Waine, T., 2014. Multiple on-line soil sensors and data fusion approach for delineation of water holding capacity zones for site specific irrigation. Soil Tillage Res. 143, 95–105. https://doi.org/10.1016/j.still.2014.06.003.
Mozejko, C.A., Francisca, F.M., 2020. Enhanced mechanical behavior of compacted clayey silts stabilized by reusing steel slag. Construct. Build. Mater. 239, 117901 https://doi.org/10.1016/j.conbuildmat.2019.117901.
Nalobile, P., Wachira, J.M., Thiong'o, J.K., Marangu, J.M., 2019. Pyroprocessing and the optimum mix ratio of rice husks, broken bricks and spent bleaching earth to make pozzolanic cement. Heliyon 5 (9). https://doi.org/10.1016/j.heliyon.2019.e02443.
Neto, J.A.D.M., Resende, D.S.D., Neto, J.T.D.S., Gouveia, A.M.C., Aguilar, M.T.P., Bezerra, A.C.S., 2014. Sterile clay pozzolans from phosphate mining. Mater. Res. 18, 230–234. https://doi.org/10.1590/1516-1439.367014.
Pappu, A., Saxena, M., Asolekar, S.R., 2007. Solid wastes generation in India and their recycling potential in building materials. Build. Environ. 42, 2311–2320. https://doi.org/10.1016/j.buildenv.2006.04.015.
Paris, J.M., Roessler, J.G., Ferraro, C.C., DeFord, H.D., Townsend, T.G., 2016. A review of waste products utilized as supplements to Portland cement in concrete. J. Clean. Prod. 121, 1–18. https://doi.org/10.1016/j.jclepro.2016.02.013.
Passos, F.L., Coelho, P., Dias, A., 2017. (Des) territórios da mineração: planejamento territorial a partir do rompimento em Mariana, MG. Cadernos Metrópole. 19 (38), 269–297. https://doi.org/10.1590/2236-9996.2017-3811.
Pavlíková, M., Zemanová, L., Pokorný, J., Záleská, M., Jankovský, O., Lojka, M., Sedmidubský, D., Pavlík, Z., 2018. Valorisation of wood chip ash as an eco-friendly mineral admixture in mortar mix design. Waste Manag. 80, 89–100. https://doi.org/10.1016/j.wasman.2018.09.004.
Puerta-Falla, G., Balonis, M., Le Saout, G., Neithalath, N., Sant, G., 2015. The influence of metakaolin on limestone reactivity in cementitious materials. In: Scrivener, K.L., Favier, A. (Eds.), Calcined Clays for Sustainable Concrete. Springer Netherlands, Dordrecht, pp. 11–19.
Rahhal, V.F., Trezza, M.A., Tironi, A., Castellano, C.C., Pavlíková, M., Pokorný, J., Irassar, E.F., Jankovský, O., Pavlík, Z., 2019. Complex characterization and behavior of waste fired brick powder-portland cement system. Materials 12, 1650. https://doi.org/10.3390/ma12101650.
Ramanathan, S., Moon, H., Croly, M., Chung, C.W., Suraneni, P., 2019. Predicting the degree of reaction of supplementary cementitious materials in cementitious pastes using a pozzolanic test. Construct. Build. Mater. 204, 621–630. https://doi.org/10.1016/j.conbuildmat.2019.01.173.
Rodier, L., Villar-Cociña, E., Ballesteros, J.M., Junior, H.S., 2019. Potential use of sugarcane bagasse and bamboo leaf ashes for elaboration of green cementitious materials. J. Clean. Prod. 231, 54–63. https://doi.org/10.1016/j.jclepro.2019.05.208.
Sakai, H., Nordfjell, T., Suadicani, K., Talbot, B., Bøllehuus, E., 2008. Soil compaction on forest soils from different kinds of tires and tracks and possibility of accurate estimate. Croat. J. For. Eng.: J. Theory Appl. For. Eng. 29, 15–27.
Salvo, M., Rizzo, S., Caldirola, M., Novajra, G., Canonico, F., Bianchi, M., Ferraris, M., 2015. Biomass ash as supplementary cementitious material (SCM). Adv Applied Ceramic 114, 3–10. https://doi.org/10.1179/1743676115Y.0000000043.
Scrivener, K.L., 2014. Options for the future of cement. Indian Concr. J. 88 (7), 11–21. July 2014.
Scrivener, K.L., John, V.M., Gartner, E.M., 2018. Eco-efficient cements: potential economically viable solutions for a low-CO_2 cement-based materials industry. Cement Concr. Res. 114, 2–26. https://doi.org/10.1016/j.cemconres.2018.03.015.
Shettima, A.U., Hussin, M.W., Ahmad, Y., Mirza, J., 2016. Evaluation of iron ore tailings as replacement for fine aggregate in concrete. Construct. Build. Mater. 120, 72–79. https://doi.org/10.1016/j.conbuildmat.2016.05.095.
Sikalidis, C., Zorba, T., Chrissafis, K., Paraskevopoulos, K.M., 2006. Ironoxide pigmenting powders produced by thermal treatment of iron solid wastesfrom steel mill pickling lines. J. Therm. Anal. Calorim. 86, 411–415. https://doi.org/10.1007/s10973-005-7168-8.
Sklivaniti, V., Tsakiridis, P.E., Katsiotis, N.S., Velissariou, D., Pistofidis, N., Papageourgiou, D., Beazi, M., 2017. J Environ Chem Eng 5, 205–213. https://doi.org/10.1016/j.jece.2016.11.042.
Soares, M.M.N.S., Poggiali, F.S.J., Bezerra, A.C.S., Figueiredo, R.B., Aguilar, M.T.P., Cetlin, P.R., 2014. The effect of calcination conditions on the physical and chemical characteristics of sugar cane bagasse ash. Rem 67 (1), 33–39. https://doi.org/10.1590/S0370-44672014000100005.
Takatsui, A., Andrade, M.F., Neisser, M.P., Barros, L.A.B., Loffredo, L.C.M., 2012. CIE L*a*b*: comparison of digital images obtained photographically manual and automatic modes. Braz. Oral Res. 26, 578–583. https://doi.org/10.1590/S1806-83242012005000025.
U.S. Geological Survey, 2017. Mineral Commodity Summaries 2017. U.S. Geological Survey, Reston, VA.
VALE, 2019. Óbitos identificados - Veja abaixo a lista de óbitos identificados pelo Instituto Médico Legal - IML, em Brumadinho. http://www.vale.com/brasil/PT/aboutvale/servicos-para-comunidade/minas-gerais/atualizacoes_brumadinho/Paginas/obitos-identificados.aspx. (Accessed 20 January 2020).
Vieira, A.P., Toledo Filho, R.D., Tavares, L.M., Cordeiro, G.C., 2020. Effect of particle size, porous structure and content of rice husk ash on the hydration process and compressive strength evolution of concrete. Construct. Build. Mater. 236 https://doi.org/10.1016/j.conbuildmat.2019.117553.
Villar-Cociña, E., Rodier, L., Savastano, H., Lefrán, M., Rojas, Moisés Frías A., 2019. Comparative Study on the Pozzolanic Activity between Bamboo Leaves Ash and Silica Fume: Kinetic Parameters. Waste Biomass Valor. https://doi.org/10.1007/s12649-018-00556-y.
Vrhovnik, P., Dolenec, T., Serafimovski, T., Dolenec, M., Šmuc, N.R., 2013. The occurrence of heavy metals and metalloids in surficial lake sediments before and after a tailings dam failure. Pol. J. Environ. Stud. 22, 1525–1538. https://doi.org/10.3906/yer-1205-1.
Yadav, A.L., Sairam, V., Muruganandam, L., Srinivasan, K., 2019. An Overview of the influences of mechanical and chemical processing on Sugarcane bagasse ash characterisation as a Supplementary Cementitious Material. J. Clean. Prod., 118854 https://doi.org/10.1016/j.jclepro.2019.118854.
Yang, L., Qiu, J., Jiang, H., Hu, S., Li, H., Li, S., 2017. Use of cemented super-fine unclassified tailings backfill for control of subsidence. Minerals 7, 216. https://doi.org/10.3390/min7110216.
Yao, G., Wang, Q., Wang, Z., Wang, J., Lyu, X., 2019. Activation of Hydration Properties of Iron Ore Tailings and Their Application as Supplementary Cementitious Materials in Cement. Powder Technology. https://doi.org/10.1016/j.powtec.2019.11.002.
Yao, G., Liu, Q., Wang, J., Wu, P., Lyu, X., 2019. Effect of mechanical grinding on pozzolanic activity and hydration properties of siliceous gold ore tailings. J. Clean. Prod. 217, 12–21. https://doi.org/10.1016/j.jclepro.2019.01.175.
Yao, G., Wang, Q., Su, Y., Wang, J., Qiu, J., Lyu, X., 2020. Mechanical activation as an innovative approach for the preparation of pozzolan from iron ore tailings. Miner. Eng. 145 https://doi.org/10.1016/j.mineng.2019.106068.
Yaprak, H., Aruntaş, H., Demir, I., Simsek, O., Durmuş, G., 2011. Effects of the fine recycled concrete aggregates on the concrete properties. Int. J. Phys. Sci. 6, 2455–2461.
Záleská, M., Pavlíková, M., Pavlík, Z., Jankovský, O., Pokorný, J., Tydlitát, V., et al., 2018. Physical and chemical characterization of technogenic pozzolans for the application in blended cements. Construct. Build. Mater. 160, 106–116. https://doi.org/10.1016/j.conbuildmat.2017.11.021.
Záleská, M., Pavlík, Z., Pavlíková, M., Scheinherrová, L., Pokorný, J., Trník, A., Svora, P., Fořt, P., Jankovský, O., Suchorab, Z., Černý, R., 2018. Biomass ash-based mineral admixture prepared from municipal sewage sludge and its application in cement composites. Clean Technol. Environ. Policy 20, 159–171. https://doi.org/10.1007/s10098-017-1465-3.
Zhang, L., Ahmari, S., Zhang, J., 2011. Synthesis and characterization of fly ash modified mine tailings-based geopolymers. Construct. Build. Mater. 25, 3773–3781. https://doi.org/10.1016/j.conbuildmat.2011.04.005.
Živica, V.R., 2004. Acidic attack of cement based materials – a review part 3: research and test methods. Construct. Build. Mater. 18, 683–688. https://doi.org/10.1016/j.conbuildmat.2004.04.030.
Zivica, V.R., Bajza, A., 2001. Acidic attack of cement based materials — a review: part 1. Principle of acidic attack. Construct. Build. Mater. 15, 331–340. https://doi.org/10.1016/S0950-0618(01)00012-5.
Zivica, V.R., Bajza, A., 2002. Acidic attack of cement-based materials—a review part 2. Factors of rate of acidic attack and protective measures. Construct. Build. Mater. 16, 215–222. https://doi.org/10.1016/S0950-0618(02)00011-9.